https://doi.org/10.5194/egusphere-2025-4015
Preprint. Discussion started: 1 September 2025

Imaging the deep carbon stocks with complex electrical conductivity

Adrián Flores Orozco[1], Jakob Gallistl[1,2], Benjamin S. Gilfedder[2], Timea Katona[1], Sven Frei[3], Peter Strauss[4], and Gunter Blöschl[5],

[1]Department of Geodesy and Geoinformation, TU Wien, Vienna, 1040, Austria
[2]Near Surface Geophysics, GeoSphere Austria, Vienna, 1190, Austria
[3]Department of Environmental Science, Wageningen University & Research, Wageningen, 9101, The Netherlands
[4]Institute for Land and Water Management Research, Federal Agency for Water Management, Scharfling, 5310, Austria
[5]Institute of Hydraulic Engineering and Water Resources Management, TU Wien, Vienna, 1040, Austria

Correspondence to: Adrian Flores Orozco (Adrian.flores-orozco@geo.tuwien.ac.at)

Abstract. Due to the limited penetration depth of standard sampling methods, mapping of soil organic carbon (SOC) is usually restricted to the top 100 cm of soils. Hence, current models underestimate SOC due to the unexplored deep carbon stocks. Moreover, standard methods only offer punctual data relying on interpolation to investigate extensive areas. We demonstrate here that subsurface images of the complex electrical conductivity (CC) can delineate the presence and geometry of SOC reaching a depth of a few tens of meters below the surface. In particular, we show that an increase the polarization effect at low frequencies (< 5 Hz) is linearly related to high concentrations of SOC. We present measurements from a catchment with silty loam soils, where the geometry of a deep carbon stock (between 4 and 6 m depth) was identified by CC images, and validated through laboratory analysis of soil samples.

1 Introduction

Soils are the largest terrestrial reservoir of organic carbon with the potential for long-term carbon storage (e.g., Panagos et al., 2013). Estimating soil organic carbon content (SOC) is therefore critically important for realistically evaluating the global C balance. Current methods primarily estimate SOC for the topsoil (0 to 100 cm depth), as they contain the largest concentrations of SOC (e.g., Harrison et al. 2011; Yost and Hartemink, 2020). However, top soils have limited potential to sequester further carbon, and it might be quickly lost to the atmosphere due to high rates of microbial respiration and soil disturbances (Button et al., 2022 and references therein). Mapping of SOC in deep soils (> 100 cm) has only been seldom addressed due to the enormous costs required for detailed deeper drilling over large areas, and analysis of the large number of samples this implies (Harrison et al. 2011; Yost and Hartemink, 2020). Furthermore, random drilling is ineffective for targeted sampling of deeper SOC layers, so any investigation of deep carbon stocks requires prior information for designing survey sampling strategies.

Geophysical methods permit the collecting of quasi-continuous information about subsurface properties in a non-invasive manner. Among electrical methods, complex conductivity (CC) has demonstrated the possibility of quantifying soil texture and hydraulic properties of the subsurface (see Binley et al., 2015 for a review) and its potential to sense changes in pore-space properties associated with biogeochemical processes (Atekwana and Slater 2009). CC provides information about the electrical

https://doi.org/10.5194/egusphere-2025-4015
Preprint. Discussion started: 1 September 2025

conductivity and capacitive properties of the subsurface, expressed in terms of its real (σ') and imaginary (σ'') components. The (real component) conductivity (σ') accounts for the migration of electrical charges along the electrolyte filling of the pore space and at the electrical double layer (EDL) formed at the grain-fluid interface; while the imaginary component (or polarization, σ'') accounts for the accumulation and polarization of charges at the EDL, which is also known as the induced polarization (IP) effect.

The CC method was initially developed for mining applications due to the high σ'' observed in the presence of iron sulfides such as pyrite (Seigel et al., 2017 for a review). Laboratory experiments have also demonstrated the sensitivity of the method to monitor the activity of iron reducers (Williams et al., 2005; Ntarlagiannis et al., 2005). Field experiments have suggested the possibility to sense not only the activity of iron reducers, but also changes in the redox-state of sediments accompanying the bioremediation of uranium contaminant plumes (Flores Orozco et al., 2011; 2013). Extensive measurements revealed the potential of the CC method to map the presence of naturally reduced zones, where organic matter at a few meters below the surface stimulated the activity of iron-reducing bacteria and resulted in the accumulation of iron sulfides (Wainwright et al., 2015).

In the absence of metallic minerals, the use of the CC method to characterize organic contaminants has been well documented (e.g., Flores Orozco et al., 2012a; Schwartz and Furman, 2012; Johansson et al., 2015). Recently, Flores Orozco et al. (2020) demonstrated the possibility of the CC method to map areas with high rates of methanogenesis, i.e., biogeochemical hot spots in municipal solid waste (MSW) landfill. The authors found that the polarization (σ'') response was related to total organic carbon. Built on these results, Katona et al. (2021) used CC measurements to delineate the geometry of carbon-turnover hotspots in peatlands. McAnallen et al. (2018) and Strobel et al. (2023) also revealed high σ''values due to an increase of organic carbon in degraded peatlands, while Ponziani et al., (2012) reported a decrease in σ'' with increasing the humification of peatlands.

To our knowledge, no study has so far addressed the identification of SOC in mineral soils using CC. This study aims at filling this knowledge gap. Our results demonstrate the potential of CC images for mapping high SOC concentrations in deep loamy soils at the catchment scale. Measurements presented here were collected in the Hydrological Open Air Laboratory (HOAL), a 66 ha catchment dedicated to understand water flow (further details in A1).Our results evidence that the CC method can be used to map organic carbon pools at varying depths; thus, permitting to design soil sampling campaigns towards the computation of more realistic organic carbon budgets.

2 Results

2.1 The electrical properties of the HOAL – imaging results at 1Hz

Figure 1 shows the CC imaging results obtained for the measurements along the exploration line E1, from which two layers can be visually identified. (1) On the top, the silty loam related to the lowest conductivity and polarization values, while (2)

https://doi.org/10.5194/egusphere-2025-4015
Preprint. Discussion started: 1 September 2025

on the bottom is found a layer with the highest conductivity ($\sigma' = 60$ mS/m) and low polarization ($\sigma'' < 0.25$ mS/m), corresponding to the underlying lignite. Figure 1 reveals that drilling cores from B1, G2 and G4 support the interpretation of the electrical images. While no groundwater was observed during the drilling of B1 and B2, the recovered sediments were often close to saturation. The high σ' values are interpreted as being caused by the contribution of both interfacial and electrolytic conduction. Due to the fine texture of clays, polarization is mainly expected at high frequencies (> 10 Hz), explaining the low σ'' values resolved for 1 Hz data (see e.g., Mendieta et al.,2021). The increase in both σ' and σ'' for the lignite at depths below 7 m is expected due to the high surface charge in organic soils, which contributes to interfacial conductivity and polarization (e.g., Shao et al., 2017; Gao et al., 2017; Katona et al., 2021).

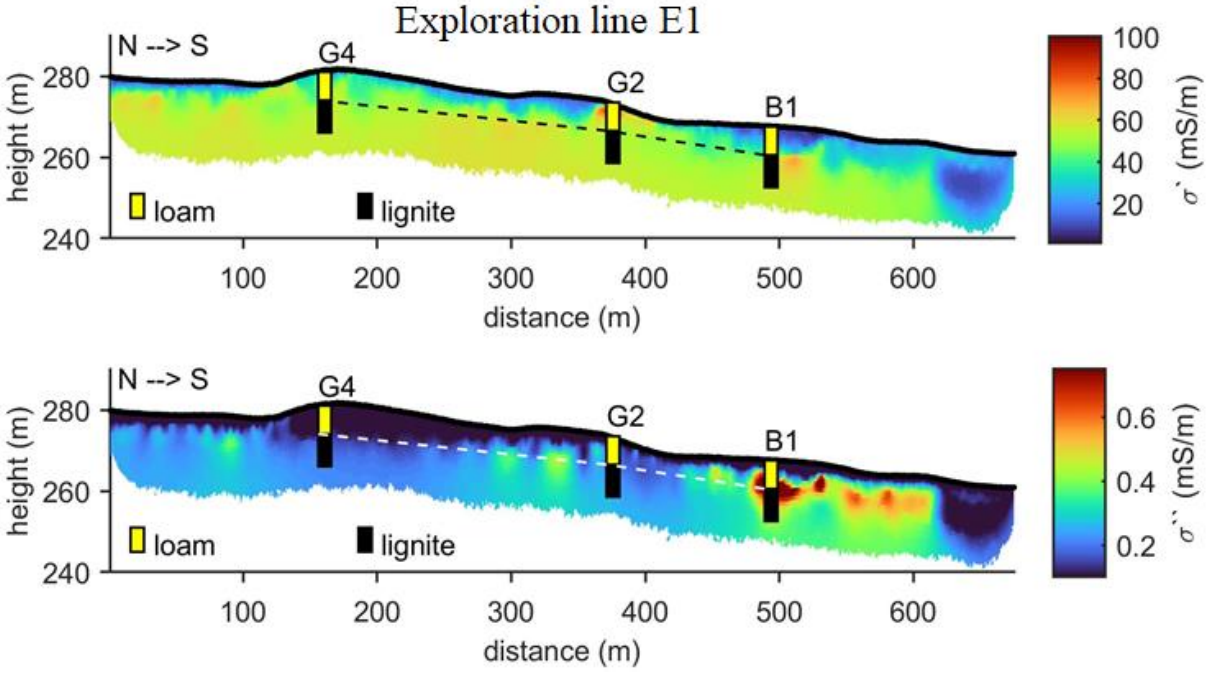

Figure 1: CC imaging results obtained for the Exploration line E1, expressed in terms of the conductivity (σ') and induced polarization (σ''). The information about lithological changes observed in soil samples extracted from existing boreholes G4 and G2, as well as the drilled borehole for this study (B1), is imposed on the electrical images for comparison. The dashed line represents the depth to the lignite layer from the linear interpolation of the borehole data.

Figure 2 shows the imaging results for parallel line SIP1. Overall, the values are consistent to those in E1. The shape of the polarizable anomaly is clearly resolved between 2 and 6 m depth at the middle of the profile, with the highest polarization (σ'' ~ 1 mS/m) at low frequencies (0.5 and 1 Hz) and a negligible response at frequencies above 7.5 Hz. In contrast, the conductivity images reveal only a layered media and no variation at the position of the polarization anomaly. Figure 2 reveals vertical changes in σ' consistent with those observed in cores from B1 and B2, with lower values ~20 mS/m) for sandy loam, and

https://doi.org/10.5194/egusphere-2025-4015
Preprint. Discussion started: 1 September 2025

higher (~50 mS/m) in clayey loam. Figure 2 also shows a shallow conductivity anomaly (between 10 and 20 m profile distance), which is only polarizable at frequencies above 10 Hz, which is indicative of a clay-rich area.

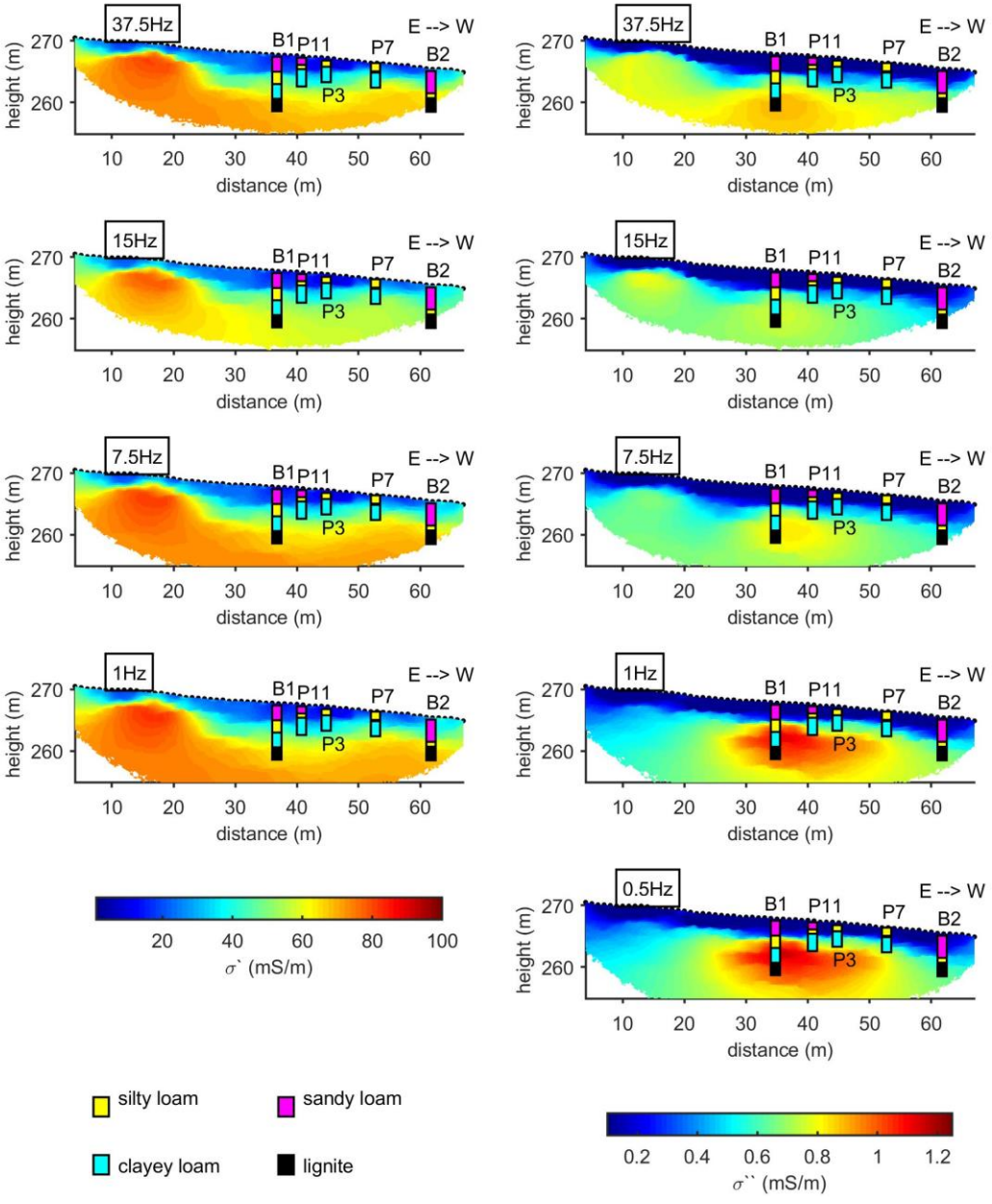

Figure 2: CC imaging results obtained for multi-frequency data collected at the line SIP1 expressed in terms of the conductivity (σ') and polarization (σ''). The information about lithological changes observed in soil samples extracted from existing piezometers (P11 and P7), as well as the drilled boreholes for this study (B1 and B1) is imposed on the electrical images for comparison.

https://doi.org/10.5194/egusphere-2025-4015
Preprint. Discussion started: 1 September 2025

2.2 The deep carbon stock: geochemical interpretation of the high electrical polarization

Figure 3 shows the laboratory analysis of the soil samples from B1 and B2 and σ' and σ''extracted from the SIP1 images at the boreholes. Such plots demonstrate that the high σ'' values resolved in B1 between 2 and 6 m depth cannot be explained by changes in the soil textural properties. The σ'' values of B1 are almost twice those of B2, although the clay content is 50% lower. The surface charge, as indicated by the CEC, also reveals consistent values of B1 and B2, with a higher increase in CEC at the lignite layer at a depth of 6 m in B1.

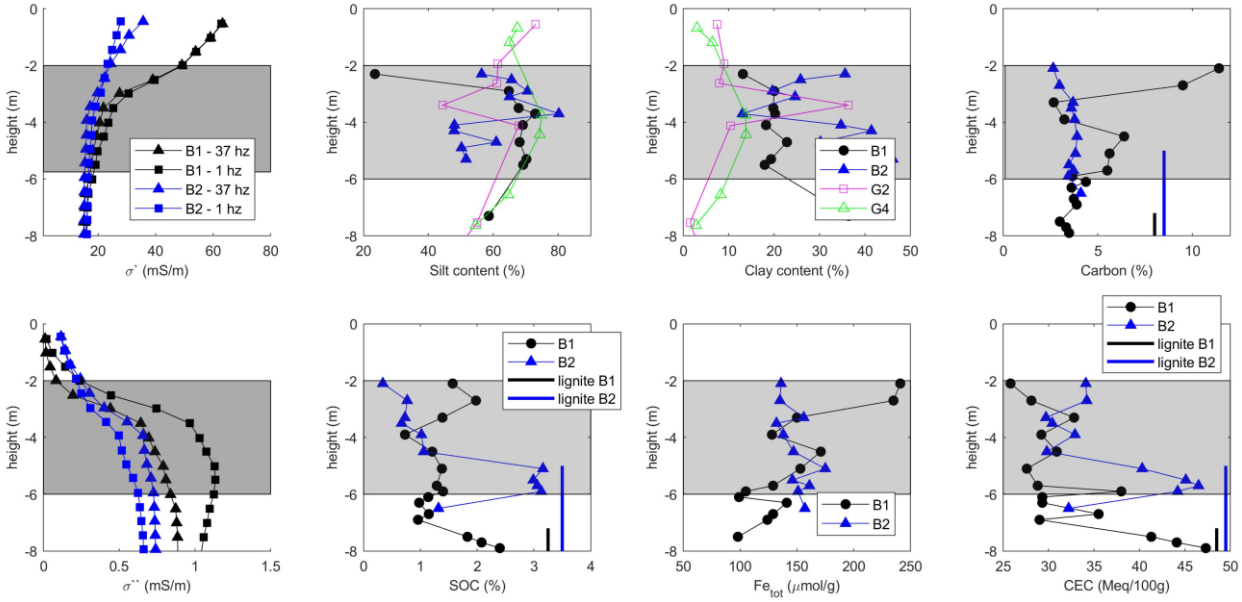

Figure 3: Comparison of the electrical (σ' and σ'') and geochemical parameters (Fe_{tot}, TOC, CEC) measured in the drilling cores (B1 and B2). Electrical parameters represent the mean values computed from pixels extracted from the inversion results of lines SIP1 at 1 Hz (solid triangles) and 37.5 Hz (solid circumferences). Textural properties in boreholes (B1 and B2) and piezometers samples are also presented for comparison. The depth to the lignite layer found at the position of B1 and B2 is indicated by the vertical lines in the plots of the SOC, Carbon and CEC data.

The polarizable anomaly (σ'') around B1 is consistent with the highest SOC and Fe_{tot} concentrations measured. In comparison, geoelectrical and geochemical parameters are much lower in B2. It might be argued that the increase in iron content enhances the electrode polarization observed in iron sulfides. However, XRD scans in our samples revealed negligible concentrations of sulfides, with the mineralogy being dominated by calcite and silicates. Hence, iron is mainly present as iron oxides, commonly related to negligible polarization at 1 Hz, with the exception of Hematite (e.g., Hubbard et al., 2014; Abdel Aal, 2014), which was also not found in our samples.

The polarizable anomaly ($\sigma'' > 1$ mS/m) is related to two carbon stocks: (1) the main one found between 2 and 3 m depth (> 2 % SOC), and (2) a deeper stock found between 4 and 6 m depth (ca 1.5 % SOC). This interpretation is supported by the

https://doi.org/10.5194/egusphere-2025-4015
Preprint. Discussion started: 1 September 2025

geochemical analysis of sediments in B1. High σ'' and SOC in B2 at 5 m depth are due to the presence of the lignite layer, which is observed at 7.2 m depth in B1.

3 Discussions

Results presented above demonstrate that soil texture properties of the HOAL vary enormously in space, so achieving a reliable characterization from a few discrete soil probes is not possible. Moreover, CC imaging results for E1 and SIP1 reveal a distinctive polarizable anomaly ($\sigma'' > 0.6$ mS/m) within 3 m and 6 m depth. At the HOAL, this is the only location at which such high polarization values have been observed. Analysis of samples collected in B1 and B2 demonstrate this anomaly is not due to buried infrastructure or changes in clay content, and can only be explained by the variations in SOC.

Mineralization of C is higher in coarse-textured soils (e.g., Hassnik, 1992), with finer grains hindering the access of soil microbes and O2 to the SOC. Additionally, clay surfaces adsorb C, forming soil aggregates that protect SOC from decomposition (Elliot, 1986). Hence, low permeable loams from the HOAL offer the best conditions to preserve SOC from O2, which can trigger the decomposition of SOC. The carbon stocks found are also favoured by the presence of iron oxides, which also play a major role in the sorption and stabilization of SOC (see Singh et al., 2018 and references therein).

Classical sampling of the top soil is limited to investigations with a maximum depth ~ 1 m; while the use of CC imaging, permitted us to map two deep carbon stocks at a high spatial resolution. However, it is still critical to use borehole data to improve the interpretation of the geophysical results. In this case, analysis of samples permitted to differentiate two separated carbon stocks from the anomaly detected with CC imaging. The deep carbon stocks found are relevant in C budgets, as these are close to the SOC average value (2.1 %) in top soils in Austria, as reported by Panagos et al. (2013).

The high polarization response at low frequencies in the presence of SOC observed here is consistent with the study of Katona et al. (2021) conducted in peatlands and with Flores Orozco et al. (2020) for measurements in municipal solid waste landfills. Gao et al. (2017; 2019) have also found evidence for the sensitivity of the method to organic carbon for measurements conducted in biochar. Similarly, Ponziani et al. (2012), McAnalen et al. (2018) and Strobel et al. (2023) reported high polarization in the presence of organic matter in peatlands but the response changed for different degrees of decomposition leading to an inconclusive $\sigma''$and SOC relationship in their study. Further analysis on the composition of the OC observed in our sample sis beyond the scope of this study.

While further research is needed to fully understand the fundamental physicochemical controls of the polarization response in presence of SOC, this study highlights the capability of the CC method to map deep carbon stocks with a spatial resolution not achievable with direct methods. Since the geochemical and geophysical measurements represent very different sampling volumes (a few grams in the soil analysis and a few m3 in the geophysical data), we refrained from a numerical comparison, focusing on highlighting the potential of the polarization images to map variations in SOC. However, quantitative estimates of SOC can be obtained from 3D electrical models of geophysical data as presented in Figure A2. Moreover, further investigations should consider CC laboratory and field monitoring experiments to better understand the geophysical response due to the sequestration and degradation of SOC.

https://doi.org/10.5194/egusphere-2025-4015
Preprint. Discussion started: 1 September 2025

4 Conclusions

We present a novel application of electrical geophysical method to resolve variations in soil organic caron (SOC) in an imaging framework. Our results demonstrate the potential of the complex conductivity imaging method to map carbon stocks in soils in a depth between 4 and 6 m. Electrical anomalies with high polarization (i.e., capacitive properties) at frequencies ≤ 1 Hz indicate high SOC, information not resolved in the electrical conductivity, which is highly sensitive to lithological changes. A suitable interpretation of the electrical images requires ground truth. Nonetheless, CC imaging results are key for an adequate design of soil sampling, yet a few samples help for the quantitative interpretation of polarization imaging results at depths not easily accessible for the collection of soil samples. In particular, the delineation of deep carbon pools is key towards obtaining reliable SOC estimates beyond the depth capabilities of current field based methods. Further research could focus on better understanding of the temporal dynamics of SOC through the application of CC monitoring.

https://doi.org/10.5194/egusphere-2025-4015
Preprint. Discussion started: 1 September 2025

5 Appendix

5.1 The Hydrological Open Air Laboratory

All data sets were collected at the HOAL, located in Petzenkirchen (Austria), which is a 66 ha observatory dedicated to understanding water-related flow and transport processes involving sediments, nutrients and microbes in small catchments (Blöschl et al., 2016). Soil cores recovered from eight boreholes distributed across the HOAL (G1 to G8 in Figure A1) reveal only silty loam soils underlain by a succession of consolidated and unconsolidated lignite. Topography variations (see Figure A1) are aligned with variations in the depth to the lignite layer between 6 m and 40 m. The silty loam soils exhibit low saturated hydraulic conductivity (< 10^{-7} m s-1) and may give rise to discrete perched aquifers, while an artesian aquifer was found below the consolidated lignite. Further details about the site can be found in Blöschl et al. (2016).

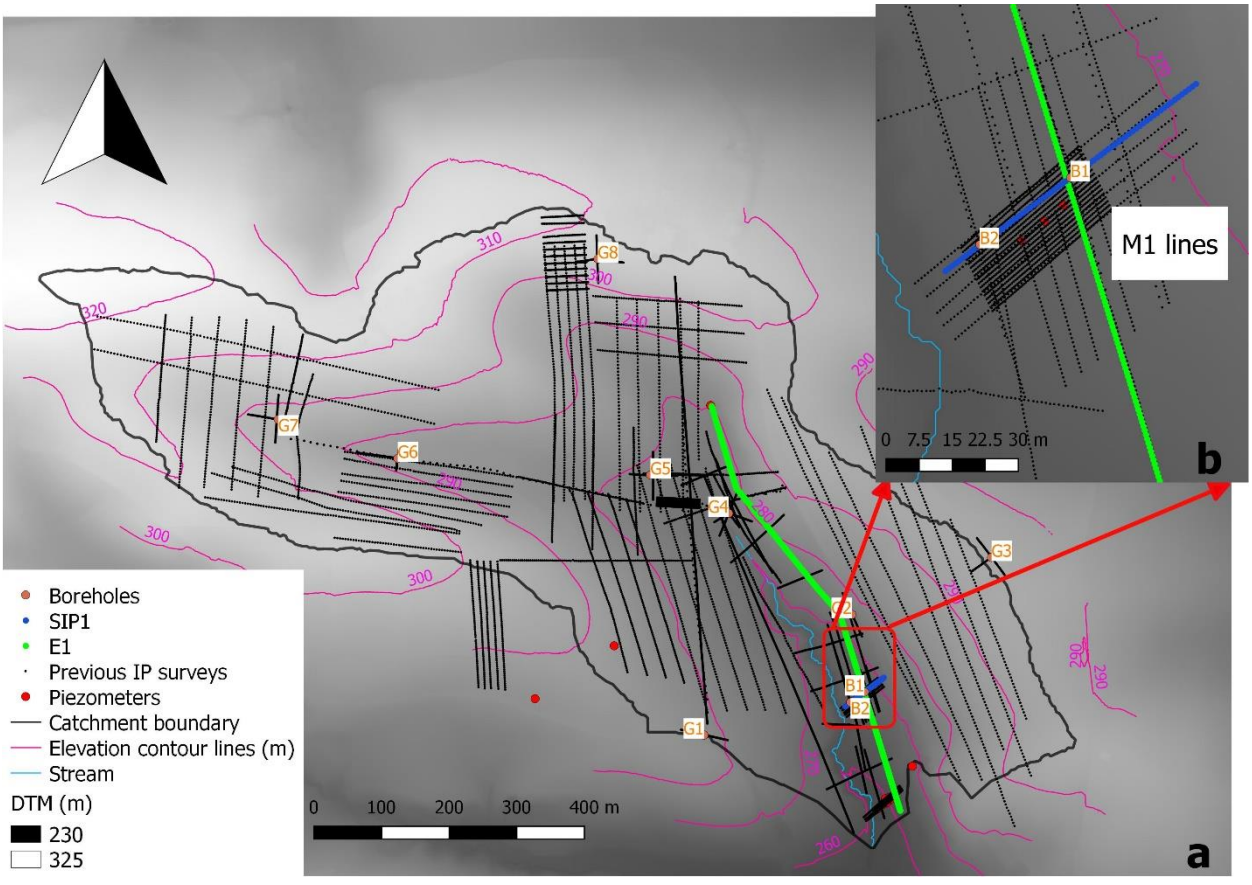

Figure A1: Existing subsurface information at the Hydrogeological Open Air Laboratory. (1a) The topography changes are indicated in the grey tones and the isolines (pink lines), available CC measurements (black lines) and boreholes (G1 to G8). The embedded plot (1b) highlights the orientation of the CC lines presented in this study: exploration results (E1 with the green line), the multi-frequency measurements (SIP1 with the blue line) and mapping measurements (M1 indicated with the black lines) as well as the boreholes B1 and B2 drilled for sampling and geochemical analysis of soil samples in the electrical anomaly.

https://doi.org/10.5194/egusphere-2025-4015
Preprint. Discussion started: 1 September 2025

5.2 The Complex Conductivity Imaging method

The CC measurements presented here were carried out with the DAS-1 instrument (Multiphase Technology, MPT) using coaxial cables to reduce distortions in the data by electromagnetic (EM) coupling (Flores Orozco et al., 2021). More than 150 lines CC have been collected in the HOAL. In this study, we present only imaging results for three data sets: M1, E1, and SIP1. E1 refers to an exploration line collected at 1 Hz using a roll-along scheme for a total of 676 electrodes and 1 m spacing between them. The SIP1 line was collected perpendicular to E1, with 64 electrodes (1 m spacing) with 10 frequencies between 0.5 and 225 Hz to gain information about the frequency-dependence of the electrical properties. The mapping data M1 comprises 27 lines using 72 electrodes in each line (further details in Appendix A2). The position and orientation of the lines is indicated in Figure A1. Erroneous measurements filtered in all data correspond to those quadrupoles associated to negative resistances and apparent resistivity readings (after modelling the numerical geometric factor for each quadrupole). Normal and reciprocal misfit analysis was conducted in representative measurements to quantify data error (see Flores Orozco et al., 2012b, 2021; 2022). We used CRTomo (Kemna, 2000) for the inversion of the data. Inversion results are presented in terms of real and imaginary components of the complex conductivity.

5.3. Ground truth: analysis of borehole sediments

During the field surveys, two boreholes (B1 and B2 in Figure A1) were drilled to a depth of 8 m for the collection of sediment samples. Sediments were immediately packed in dry ice to avoid chemical transformations. Soil chemical analysis was performed after the samples were freeze-dried and milled in an agate ball mill. Total carbon was measured by combustion using a Thermo Quest CN element analyser at the Bayreuth Keylab Experimental Biogeochemistry. Reactive iron (Fe) was determined on samples after extraction by 1M HCl. The solution was filtered (0.45 µm) and analysed for total Fe photometrically using the phenanthroline method (Wallmann et al., 1993; Tamura et al., 1974). The cations exchange capacity (CEC) was determined with ICP-OES using standard methods, except that Fe and Mn were also included in the CEC calculation in addition to the base cations. The inorganic carbon content was measured using the method described by Horváth et al., (2005) with replicate RSDs of core samples ranging from 0.8 to 2 %. The SOC carbon content is the total carbon minus inorganic carbon content. Grain sizes of sediments obtained in B1 and B2, as well as from previously drilled boreholes G2, and G4, and from four piezometers (see Figure A1) were measured by sieve analysis. Groundwater electrical conductivity (EC) measured in the piezometers was about 400 mS/m during the measurement campaign.

Here we present the geometry of the high polarizable anomaly resolved from time-domain induced polarization measurements along the 27 lines corresponding to the survey M1. Erroneous measurements filtered in all data correspond to those quadrupoles associated to negative resistances and apparent resistivity readings (after modelling the numerical geometric factor for each quadrupole). Reciprocal readings were collected in exemplary lines for statistical analysis of the misfit between normal and

https://doi.org/10.5194/egusphere-2025-4015
Preprint. Discussion started: 1 September 2025

reciprocal to quantify data error using the approach by Flores Orozco et al., (2012b, 2021; 2022). We used CRTomo (Kemna, 2000) for the inversion of the data. Chargeability measurements were linearly converted to 1 Hz apparent phase values using the approach described elsewhere (Kemna, 2000; Flores Orozco et al., 2021). Inversion results are presented in terms of the imaginary component of the complex conductivity (σ'').

5.2 The geometry of the deep carbon stock

Figure A2 shows the extension of the polarization (σ'') anomaly resolved at 4 m depth as obtained from the interpolation of the complex conductivity imaging results from the inversion of all mapping lines referred to as M1. The mapping M1 consists of 32 lines, namely: 5 long and 17 short lines parallel to the stream direction (roughly N-S), as well as 5 long and 5 short lines perpendicular to them (roughly W-E). Long lines have a separation of 5 m between them and were carried out using 72 electrodes in each with 1 m spacing between electrodes; whereas short lines have 1 m separation between them, each with 72 electrodes and a spacing of 0.5 m. The data were inverted for each independent line using CRTomo using the same methodology as the one used for the processing and inversion of lines E1 an SIP1. Nonetheless, the 3D inversion of all M1 lines was also conducted with other inversion algorithms in actual 3D (data not shown) revealing consistent results with the Figure A2 presented below. Considering that the data was collected without measurements a using electrodes placed in different lines, we decided here to work only with 2D inversion.

The geometry of the carbon stock at 4 m depth presented in A2 correspond to the high polarization values ($\sigma`` > 900\ \mu$S/m) extracted from the inversion of the M1 data. These values are consistent to those observed in the E1 and SIP lines (Figure 2 and 3). The map presented in Figure A2 reveals that the carbon stock extends towards the northwest from the drilled boreholes B1, where the high organic carbon content was measured in soil samples (Figure 4). The map presented in Figure A2 can be used to guide further drilling for the collection of soil samples.

https://doi.org/10.5194/egusphere-2025-4015
Preprint. Discussion started: 1 September 2025

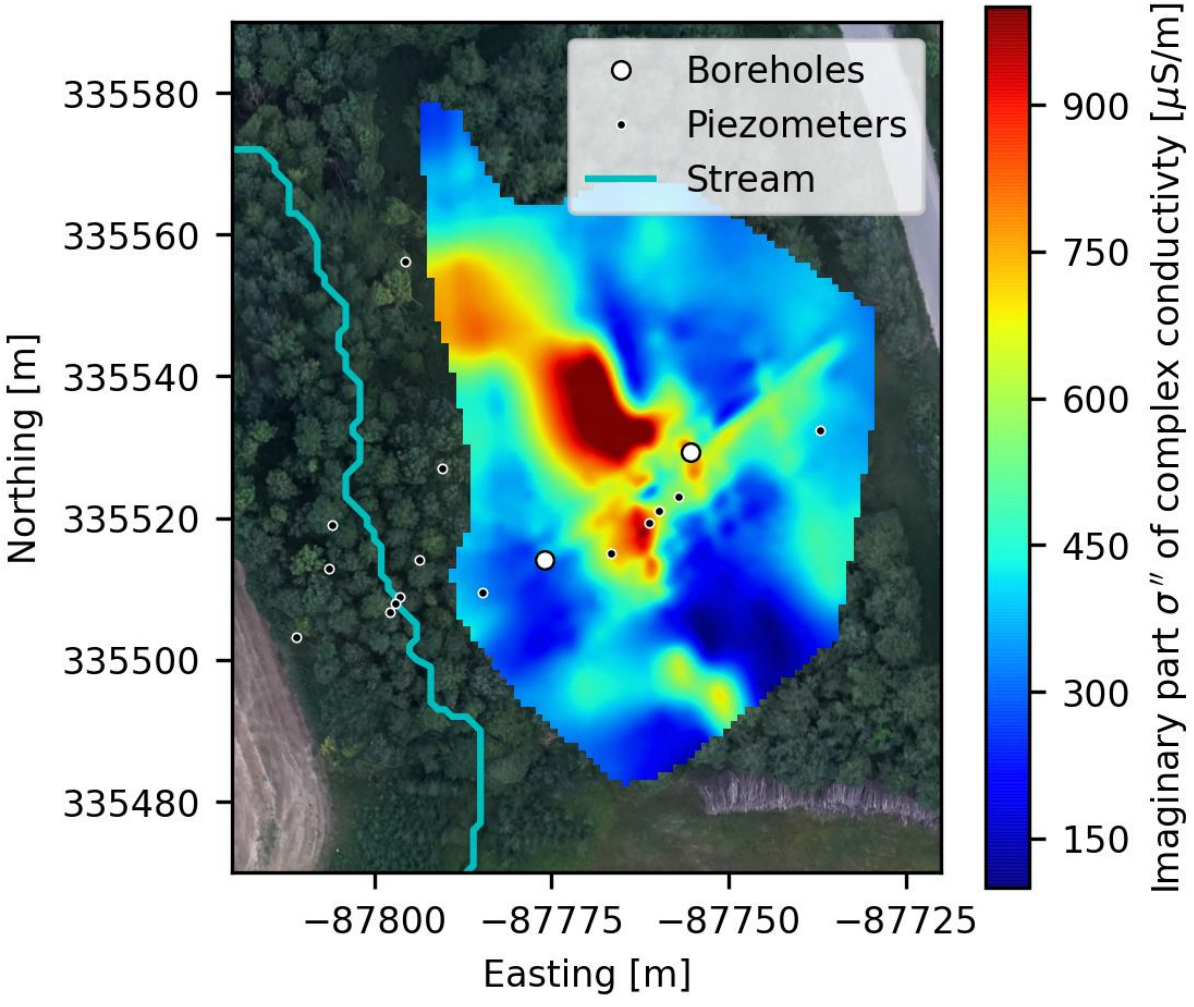

Figure A2. Geometry of the deep carbon stock (at 4 m depth) given by the anomalous high induced polarization values (σ'' > 1 mS/m)

https://doi.org/10.5194/egusphere-2025-4015
Preprint. Discussion started: 1 September 2025

6 Data availability

Data presented here are available at the repository of the TU Wien with the digital object identifier (DOI): https://doi.org/10.48436/5h7jb-26w42

7 Author contribution

AFO designed the experiments, while JG and TK carried out field data, with laboratory analysis of samples conducted by BG. AFO conducted the Data Curation, Formal Analysis, Methodology and Visualization. AFO, GB, PS and SF were in charge of Resources. AFO prepared the manuscript with contributions from all co-authors.

References

Abdel Aal, G.Z., Atekwana, E.A. & Revil, A. 2014. Geophysical signatures of disseminated iron minerals: A proxy for understanding subsurface biophysicochemical processes. Journal of Geophysical Research: Biogeosciences, 119(9), pp.1831-1849.

Atekwana, E.A. and Slater, L.D., 2009. Biogeophysics: A new frontier in Earth science research. Reviews of Geophysics, 47(4).

Binley, A., Hubbard, S.S., Huisman, J.A., Revil, A., Robinson, D.A., Singha, K. & Slater, L.D. 2015. The emergence of hydrogeophysics for improved understanding of subsurface processes over multiple scales. Water resources research, 51(6), pp.3837-3866.

Blöschl, G., A. P. Blaschke, M. Broer, C. Bucher, G. Carr, X. Chen, A. Eder, M. Exner-Kittridge, A. Farnleitner, A. Flores-Orozco, P. Haas, P. Hogan, A. Kazemi Amiri, M. Oismüller, J. Parajka, R. Silasari, P. Stadler, P. Strauß, M. Vreugdenhil, W. Wagner and M. Zessner (2016) The Hydrological Open Air Laboratory (HOAL) in Petzenkirchen: a hypothesis-driven observatory, Hydrology and Earth System Sciences, 20, 227-255, doi:10.5194/hess-20-227-2016.

Button, E.S., Pett-Ridge, J., Murphy, D.V., Kuzyakov, Y., Chadwick, D.R. & Jones, D.L. (2022). Deep-C storage: Biological, chemical and physical strategies to enhance carbon stocks in agricultural subsoils. Soil Biology and Biochemistry, 170, p.108697.

Elliott, E., 1986. Aggregate structure and carbon, nitrogen, and phosphorus in native and cultivated soils. Soil science society of America journal, 50(3), pp.627-633.

Flores Orozco, A., Williams, K.H., Long, P.E., Hubbard, S.S. and Kemna, A., 2011. Using complex resistivity imaging to infer biogeochemical processes associated with bioremediation of an uranium-contaminated aquifer. Journal of Geophysical Research: Biogeosciences, 116(G3).

https://doi.org/10.5194/egusphere-2025-4015
Preprint. Discussion started: 1 September 2025

Flores Orozco, A., Williams, K.H. and Kemna, A., 2013. Time-lapse spectral induced polarization imaging of stimulated uranium bioremediation. Near Surface Geophysics, 11(5), pp.531-544.

Flores-Orozco, A., Gallistl, J., Steiner, M., Brandstätter, C. and Fellner, J., 2020. Mapping biogeochemically active zones in landfills with induced polarization imaging: The Heferlbach landfill. Waste Management, 107, pp.121-132.

Flores Orozco, A., Micić, V., Bücker, M., Gallistl, J., Hofmann, T. and Nguyen, F., 2019. Complex-conductivity monitoring to delineate aquifer pore clogging during nanoparticles injection. Geophysical Journal International, 218(3), pp.1838-1852.

Flores Orozco, A., Velimirovic, M., Tosco, T., Kemna, A., Sapion, H., Klaas, N., Sethi, R. and Bastiaens, L., 2015. Monitoring the injection of microscale zerovalent iron particles for groundwater remediation by means of complex electrical conductivity imaging. Environmental science & technology, 49(9), pp.5593-5600.

Gao, Z., Haegel, F.H., Huisman, J.A., Esser, O., Zimmermann, E. and Vereecken, H.: Spectral induced polarization for the characterisation of biochar in sand, Near surface geophysics, 15(6), pp.645-656.

Gao, Z., Haegel, F.H., Esser, O., Zimmermann, E., Vereecken, H. and Huisman, J.A.: Spectral induced polarization of biochar in variably saturated soil, Vadose zone journal, 18(1), pp.1-13.

Hassink, J.: Effects of soil texture and structure on carbon and nitrogen mineralization in grassland soils, Biology and Fertility of Soils, 14, pp.126-134.

Horváth, B., Opara-Nadi, O. and Beese, F.: A simple method for measuring the carbonate content of soils, Soil Sci. Soc. Am. J., 69: 1066-1068. doi.org/10.2136/sssaj2004.0010

Hubbard, C.G., West, L.J., Rodriguez-Blanco, J.D. and Shaw, S.: Laboratory study of spectral induced polarization responses of magnetite—Fe 2+ redox reactions in porous media, Geophysics, 79(1), pp.D21-D30.

Johansson, S., Fiandaca, G., and Dahlin, T.: Influence of non-aqueous phase liquid configuration on induced polarization parameters: Conceptual models applied to a time-domain field case study, Journal of Applied Geophysics 123 (2015): 295-309.

Katona, T., Gilfedder, B.S., Frei, S., Bücker, M. and Flores-Orozco, A.: High-resolution induced polarization imaging of biogeochemical carbon turnover hotspots in a peatland, Biogeosciences, 18(13), pp.4039-4058.

Mendieta, A., Jougnot, D., Leroy, P. and Maineult, A.: Spectral induced polarization characterization of non-consolidated clays for varying salinities—An experimental study, Journal of Geophysical Research: Solid Earth, 126(4), p.e2020JB021125.

McAnallen, L., Doherty, R., Donohue, S., Kirmizakis, P. and Mendonça, C.: Combined use of geophysical and geochemical methods to assess areas of active, degrading and restored blanket bog, Science of the Total Environment, 621, pp.762-771.

Ntarlagiannis, D., Williams, K.H., Slater, L. and Hubbard, S.: Low-frequency electrical response to microbial induced sulfide precipitation, Journal of Geophysical Research: Biogeosciences, 110(G2).

Panagos, P., Hiederer, R., Van Liedekerke, M. and Bampa, F.: Estimating soil organic carbon in Europe based on data collected through an European network, Ecological Indicators, 24, pp.439-450.

Ponziani, M., Slob, E.C., Vanhala, H. and Ngan-Tillard, D.J.M.: Influence of physical and chemical properties on the low-frequency complex conductivity of peat, Near Surface Geophysics, 10(6), pp.491-501.

https://doi.org/10.5194/egusphere-2025-4015
Preprint. Discussion started: 1 September 2025

Schwartz, N. and Furman, A.: Spectral induced polarization signature of soil contaminated by organic pollutant: Experiment and modelling, Journal of Geophysical Research: Solid Earth, 117(B10).

Shao, Z., Revil, A., Mao, D. and Wang, D.: Induced polarization signature of coal seam fires, Geophysical Journal International, 208(3), pp.1313-1331.

Seigel, H., Nabighian, M., Parasnis, D.S. and Vozoff, K.: The early history of the induced polarization method, The Leading Edge, 26(3), pp.312-321.

Singh, M., Sarkar, B., Sarkar, S., Churchman, J., Bolan, N., Mandal, S., Menon, M., Purakayastha, T.J. and Beerling, D.J.: Stabilization of soil organic carbon as influenced by clay mineralogy, Advances in agronomy, 148, pp.33-84.

Strobel, C., Dörrich, M., Stieff, E.H., Huisman, J.A., Cirpka, O.A. and Mellage, A.: Organic matter matters—The imaginary conductivity of sediments rich in solid organic carbon, Geophysical Research Letters, 50(23), p.e 2023GL104630.

Tamura, H., Goto, K., Yotsuyanagi, T., and Nagayama, M.: Spectrophotometric determination of iron (II) with 1, 10phenanthroline in the presence of large amounts of iron (III). Talanta, 21, 314–318

Wallmann, K., Hennies, K., König, I., Petersen, W., and Knauth, H.D.: New procedure for determining reactive Fe(III) and Fe(II) minerals in sediments, Limnology and Oceanography, 38.

Wainwright, H.M., Flores Orozco, A., Bücker, M., Dafflon, B., Chen, J., Hubbard, S.S. and Williams, K.H.: Hierarchical Bayesian method for mapping biogeochemical hot spots using induced polarization imaging, Water Resources Research, 52(1), pp.533-551.

Williams, K.H., Ntarlagiannis, D., Slater, L.D., Dohnalkova, A., Hubbard, S.S. and Banfield, J.F.: Geophysical imaging of stimulated microbial biomineralization, Environmental science & technology, 39(19), pp.7592-7600.

Yost, J.L. and Hartemink, A.E., 2020. How deep is the soil studied–an analysis of four soil science journals. Plant and soil, 452, pp.5-18.